Electrochemical performance of gold nanoparticles decorated on Multi-walled Carbon Nanotube (MWCNT) Screen-printed Electrode (SPE)

Fitria Yunita Dewi[1], *Soni Tri* Cahyono[1], *Fakhri* Hilmi[1], *Afiten Rahmin* Sanjaya[2], *Dian Wulan* Hastuti[1], *Nur Intan* Pratiwi[1], *Harry Kusuma* Aliwarga[3], *Prawito* Prajitno[1], *Tribidasari Anggraningrum* Ivandini[2], and *Djati* Handoko[1,*]

[1]Department of Physics, Faculty of Mathematics and Natural Sciences (FMIPA), Universitas Indonesia, Depok 16424, Indonesia
[2]Department of Chemistry, Faculty of Mathematics and Natural Sciences (FMIPA), Universitas Indonesia, Depok 16424, Indonesia
[3]UMG Idealab, Indonesia

Abstract. The modification of the multi-walled carbon nanotube screen-printed electrode (MWCNT/SPE) with gold nanoparticles (AuNP) was achieved through drop-casting method utilizing gold nanoparticles synthesized via the Turkevich method. The combination of nanomaterial based on carbon (multi-walled carbon nanotubes) and the noble metal (gold nanoparticles) aims to exploit the synergistic benefits of the two materials in electrochemical measurement. Electrochemical performance was evaluated through techniques including cyclic voltammetry and electrochemical impedance spectroscopy (EIS). The results indicated an increase in the electroactive surface area of the modified working electrodes compared to the unmodified ones. This increase in electroactive surface area can be attributed to the successful decoration of AuNP, which facilitates greater surface interactions and improved electron transfer kinetics, crucial for efficient catalytic reactions. The decoration of AuNP also makes sure that the electrode will have good biocompatibility for future bioanalytical applications. This investigation's main goal was to determine the effects of the AuNP modification methods to the carbon electrode's electroactive surface area for further contributing to the development of efficient label-free sensing platforms for diverse applications in biosensing.

Keywords. Electrochemistry, gold nanoparticle, multi-walled carbon nanotube, sensor, screen-printed electrode

* Corresponding author: djati.handoko@ui.ac.id

1 Introduction

1.1 Electrochemical sensing with Screen-printed Electrode (SPE)

Electrochemical sensing is a technique that utilizes the principles of electrochemistry to detect and quantify chemical or biological analytes (substances of interest) in a sample. These detections and quantifications can be seen in some of these studies, such as the sensing of capsaicin[1], bisphenol [2], ascorbic acid [3], and heavy metal ions in water for instances, zinc (Zn(II)), lead (Pb(II)), and copper (Cu(II)) [4]. Recently, modern sensing systems have benefited from advances in microelectronic and microengineering, mainly through the manufacturing of even smaller sensors with more sensitivity and more selectivity, and with lower production and maintenance costs. Conventional electrode in electrochemical sensing technology has some disadvantages such as their need for a large amount of analyte for determination [5], surface contamination and passivation, tedious cleaning process and difficulty in modifying the electrode with larger area. One way to achieve this smaller sensor in electrochemical sensing is by utilizing screen printed electrode (SPE). SPEs are basically a miniaturized electrochemical cell that consists of three electrodes, which are working electrode (WE), reference electrode (RE) and counter electrode (CE), printed on a solid substrate. The small size of screen-printed electrodes (usually in dimension of 34 mm × 10 mm × 0.5 mm) leads to the minimization of the size of the working electrode, the low cost, the decrease in the analyte amount required for determination (only 50 μL), and minimal waste production. SPEs have been demonstrated to be very versatile, since they are suitable for various designs, can be made from various substances, and can readily be modified by different biological components such as synthetic diagnostic elements, enzymes, DNA, and antibodies [6].

1.2 Multi-walled Carbon Nanotubes (MWCNT) and gold nanoparticles (AuNP) modification

Several modifications have been made to improve SPE's analytical properties employing numerous kinds of nanomaterials, structures, and synthetic substances, which have produced quite successful results in several investigated situations [7]. Various carbon-based substances such as carbon black (CB), carbon nanotubes (CNTs), graphene (Gr), and metallic nanoparticles (Au and Ag), along with magnetic beads (MBs) have been utilized for SPE modification. Modified nanomaterials can have similar properties with biological diagnostic elements like proteins and DNA, whose combination can produce synergistic effects that provide unpredicted benefits [8]. Nanomaterials play an important role in the development of electrochemical sensing, since modification of the sensor with nanomaterials can greatly improve the analytical properties of the sensors including sensitivity and selectivity, while simultaneously improving stability and maintaining a low limit of detection (LOD) [9]. The most straightforward approach for enhancing SPEs involves depositing the modifying agent onto the working electrode (WE) surface, a process supported by the flat nature of its surface.

Carbon nanotubes (CNT) have good conductivity, chemical stability, large specific area, and are capable of minimizing surface fouling and accelerating the electrochemical reactions rate [2]. There are many applications of carbon nanotubes, usually multiwalled carbon nanotubes (MWCNT), such as in batteries, nanoelectronic devices, and as nanomaterial modifiers of the surfaces of electrochemical sensors.

For the application of biosensors, gold nanoparticles (AuNPs) play a crucial role and have been widely used as they are one of the most impressive metal nanoparticles [10]. AuNPs are desirable materials for biorecognition applications because they are readily conjugated with

biomolecules and retain the biochemical activity of tagged biomolecules. AuNPs have been widely exploited as sensitive tracers for biomolecular recognition events due to their detectable electron dense core, high surface to volume ratio, and tuneable electrochemical activity [11].

The modification of gold nanoparticles on to the electrode surface can be done in various ways, such as electrodeposition, direct deposition/drop-casting, and ink mixing. Among these approaches, the drop-casting method has been the easiest and simplest approach for nanomaterials deposition [12] and will be the modification strategy in this study.

2 Materials and method

2.1 Reagents

Tetrachloroauric(III) acid trihydrate ($HAuCl_4.3H_2O$ 99.9%), trisodium citrate ($Na_3C_6H_5O_7$), monopotassium phosphate (KH_2PO_4), dipotassium phosphate (K_2HPO_4) were all purchased from Merck, Singapore. Phosphate buffered saline (PBS) solution (0.1 M and pH 7) was prepared by dissolving KH_2PO_4 and K_2HPO_4 in distilled water. Potassium ferricyanide $K_3[Fe(CN)_6]$ as the redox probe, isopropanol and sulfuric acid (H_2SO_4) were purchased from Smart Lab, Indonesia.

2.2 Apparatus

In this study, we used commercially available screen-printed electrodes as sensors from Metrohm DropSens, Spain. The first one is screen-printed carbon electrode (SPCE ref: 110) and the second type is screen-printed carbon electrode modified with carboxyl functionalized multiwalled carbon nanotubes (SPCE/MWCNTs-COOH ref:110CNT). The working electrode of the prior is made of carbon (ref. 110) while the latter are modified by carboxyl functionalized multiwalled carbon nanotubes (ref. 110CNT). Both types have a carbon counter electrode, and a silver reference electrode. Compared with the SPCE, SPCE/MWCNTs-COOH is expected to provide a greater sensitivity and a broader linear range. All the electrochemical measurements were performed with potentiostat/galvanostat CS310M model from Corrtest Instrument. The electrodes were connected to potentiostat using DropSens Connector.

2.3 Preparation of the sensors

SPCEs are prepared through steps of pre-treatment. The electrodes were rinsed in distilled water to ensure the surface was free from contamination. The surface then continued to be activated with cyclic voltammetry (CV) in 0.1 M sulfuric acid in a potential range of -1 to 1 V for 15 cycles and also in PBS solution in a potential range of 0 to 0.8 V for 20 cycles. This activation ensures that there are hydroxyl, carbonyl, and carboxyl functional groups generated at the surface and can be utilized to form hydrogen and/or covalent bonds, which are useful for interacting with Au nanoparticles[13].

2.4 Synthesis of gold nanoparticles

Gold nanoparticles were prepared using the Turkevich method [14]. For further use, 50 mL of 5 mM $HAuCl_4$ and 50 mL of 60 mM sodium citrate were prepared for stock solutions. All the solutions used distilled water as solvent. Other variations of concentration (1 mM $HAuCl_4$ and 20 mM $Na_3C_6H_5O_7$) were prepared by diluting the stock solutions in

distilled water. The synthesis of gold nanoparticles was carried out by heating 50 mL of 1 mM $HAuCl_4$ solution until boiling point in a beaker covered tightly with aluminium foil with constant stirring at 300 rpm using a magnetic stirrer. After that, 5 mL of trisodium citrate solution of 20 mM and 60 mM was added to the above solution (in a separate beaker for creating two variations of AuNP) with constant heating and stirring at 300 rpm for 15 minutes. The nanoparticle suspension was then continuously stirred at 300 rpm and cooled down to room temperature. This process was carried out in a fume hood.

Two nanoparticle suspension variations from different ratio of chloroauric acid and citrate are called Au 1-20 (for ratio 1:20) and Au 1-60 (for ratio 1:60). Both suspensions were analysed with UV-Vis Spectroscopy to find the estimated distribution of gold nanoparticle's diameter for each variation. Generally, as the size increases, absorption peak in the spectrum shifts to longer wavelength. The diameter and concentration can be calculated from the formula below [15].

$$d = \frac{ln\left(\frac{\lambda_{spr} - \lambda_0}{L_1}\right)}{L_2} \tag{1}$$

$$\mathrm{N} = \frac{A_{450} \times 10^{14}}{d^2\left[-0.295 + 1.36\exp\left(-\left(\frac{d - 96.8}{78.2}\right)^2\right)\right]} \tag{2}$$

Here λ_{spr} is the peak position from spectra data, and the fit parameters determined from the theoretical values for d > 25 nm ($\lambda_0 = 512$, $L_1 = 6.53$, $L_2 = 0.0216$). A_{450} is the absorbance at $\lambda = 450$ nm, and d is the particle diameter in nanometer.

The modification of the sensors was carried out by drop-casting each suspension (10 uL in volume) with micropipette on to the surface of the working electrode only. The electrode was then left to dry for a day.

2.5 Determination of electroactive surface area and charge transfer resistance

The electroactive surface area was measured by performing cyclic voltammetry on each sensor sample using 50 µL of 20 mM $K_3[Fe(CN)_6]$ as a redox probe in a prepared PBS solution with scan rates of 25, 50, 100, 125, 150, and 200 mV/s in the potential region of -0.5 V to 1 V (vs. Ag as the reference electrode/RE). To find the estimated electroactive surface area, we can fit linear regression of current peaks versus square root of scan rate variations according to the following equation.

$$\mathrm{i_p} = 0.4463\left(\frac{n^3F^3}{RT}\right)^{\frac{1}{2}} AC^0(D_0v)^{1/2} \tag{3}$$

Where i_p is the measured peak current in voltammogram (A), n is the number of electrons transferred in the reaction, F is Faraday's constant (96485 C/mol), C is the molar concentration of the redox species (20 mM), D is the diffusion coefficient of the redox species (± 7.3 cm^2/s), R is the gas constant (8.3144 J/mol K), T is the temperature (K), v is the scan rate (V/s) and A is the electroactive surface area (cm^2).

The results from CV will also be convinced from electrochemical impedance spectroscopy (EIS) measurements to analyze the charge transfer impedance (R_{ct}) of each sensor.

3 Results

3.1 Nanoparticles size and concentration

To ensure that gold nanoparticles were really formed after the synthesis process, UV-Vis spectroscopy was carried out. It can be seen from the spectra results that the absorbance peak is in the range of 520 nm to 600 nm, which indicates the formation of gold nanoparticles[16]. The size and concentration of two variations of gold nanoparticle suspension were calculated with Equation (1) and Equation (2). The results are shown in Table 1.

Table 1. Diameter and concentration of AuNP synthesized with Turkevich method.

Chloroauric acid Concentration	Trisodium citrate concentration	AuNP Diameter (mm)	AuNP Concentration (x10^{10} particles/mL)
1 mM	20 mM	42.2 ± 8.7	6.01 ± 4.6
1 mM	60 mM	56.9 ± 6.3	1.68 ± 0.6

From the results, we can see that Au 1-20 has smaller diameter than Au 1-60, which is also consistent with the colour of the suspension, where the smaller AuNP appeared reddish while the other appeared bluish (Fig. 1).

(a)

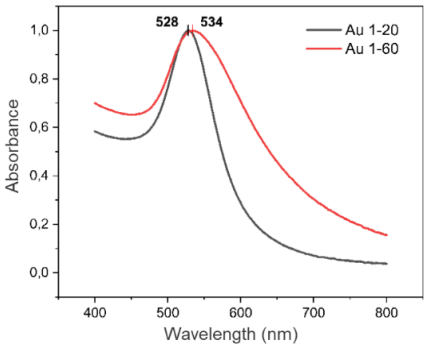

(b)

Fig. 1. (a) Gold nanoparticle suspension Au 1-20 (reddish) and Au 1-60 (bluish), (b) UV-Vis spectra of Au 1-20 and Au 1-60.

3.2 Electroactive surface area

All sensors, including SPCE, SPCE/MWCNT without modification, SPCE/MWCNT/Au1-20, and SPCE/MWCNT/Au1-60, were characterized by CV with scan rate variations. Figure 2 shows that the peak current during oxidation or reduction process increases with the scanning rate. It proves Equation (3) that there is a linear positive

relationship between square root scan rate and peak current. In addition, physically, the higher the scanning rate, the faster the analyte can diffuse to the electrode surface so that more species are oxidized or reduced which causes a higher current response [17].

Calculated from linear regression fitting, it was found that the active surface area of the bare SPCE sensor was 0.108 ± 0.001 cm^2 and the area of MWCNT-decorated SPCE or SPCE/MWCNT sensor was 0.136 ± 0.002 cm^2. The bare SPCE surface area is smaller than the geometric area of the working electrode in SPCE which is 0.126 cm^2. So, the active surface area is only 85.95 % of the geometric area of the working electrode. This might be due to the uneven surface of the SPCE and the inactive side due to the fabrication process which uses a polymeric binder from PVC.

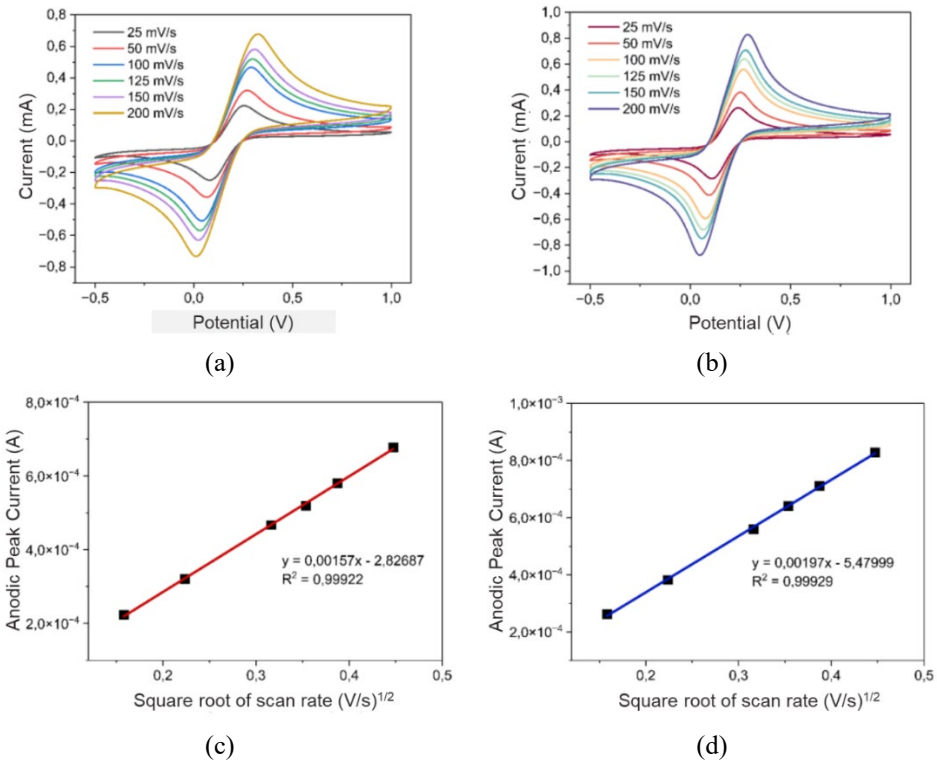

Fig. 2. Voltammogram of (a) bare SPCE, (b) SPCE/MWCNT, and linear regression fitting of current peak vs. square root of scan rate from (c) bare SPCE, (d) SPCE/MWCNT.

For the modified sensors with AuNP, the electroactive surface area was also calculated from the linear regression fitting. Figure 3 shows that the voltammogram results electrochemically are in accordance with the unmodified sensors where the current peak also increases with the scan rate. The surface area of SPCE/MWCNT/Au 1-20 sensor was found to be 0.250 ± 0.007 cm^2 and that of SPCE/MWCNT/Au 1-60 was 0.127 ± 0.001 cm^2. The AuNP modification was expected to increase the electroactive surface area of the sensor and was proven in the SPCE/MWCNT/Au 1-20 sensor where the area increase is almost twice the geometric area of WE. However, on the SPCE/MWCNT/Au 1-20 sensor, the calculated surface area decreased compared to the geometric area or WE and did not show any improvement after modification. This can be caused by the agglomeration of the deposited nanoparticles as a result of the drawbacks of the drop-cast method. Agglomerated

nanoparticles can avoid the increase in electroactive area and even reduce the electroactive sites. Apart from that, the SPCE/MWCNT/Au 1-20 sensor has a higher nanoparticle concentration, allowing more nanoparticles to be successfully deposited, thus increasing the electroactive surface area. The comparison of the active surface area of all sensors can be seen in the Table 2.

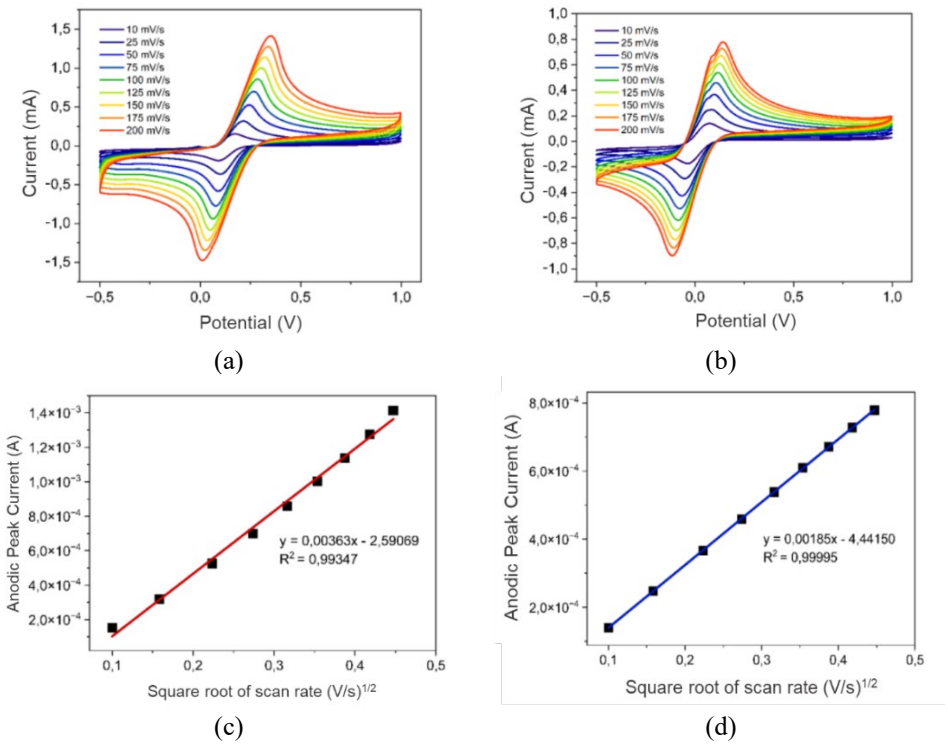

Fig. 3. Voltammogram of (a) SPCE/MWCNT/Au 1-20, (b) SPCE/MWCNT/Au 1-60, and linear regression fitting of current peak vs. square root of scan rate from (c) SPCE/MWCNT/Au 1-20, (d) SPCE/MWCNT/Au 1-60.

Table 2. Electroactive surface area for each sensor.

Sensor	Electroactive surface area (cm^2)	Ratio of electroactive surface area to WE geometric area (0.126 cm^2)
SPCE	0.108 ± 0.001	85.95 %
SPCE/MWCNT	0.136 ± 0.002	107.85 %
SPCE/MWCNT/Au 1-20	0.250 ± 0.007	198.73 %
SPCE/MWCNT/Au 1-60	0.127 ± 0.001	101.28 %

Overall, the peak current and electroactive surface areas of sensors decorated with MWCNT are always higher than that of bare SPCE. So, MWCNT modification is proven to improve the conductivity of the sensors. The highest area was achieved in the

SPCE/MWCNT/Au 1-20 modification, which also implies that the conductivity must be the highest among all sensors since there are more active sites for the oxidation and reduction processes to occur. So, the deposition of gold nanoparticles can also increase the conductivity as long as there is an appropriate amount of concentration and fewer agglomeration effects that could take place.

For comparison, Table 3 shows the calculated electroactive surface area obtained from other studies that also utilized AuNP modification on screen-printed carbon electrodes. All the other studies have successfully increased the electroactive surface area of the bare SPCE. However, many of them involve relatively lengthy preparation processes due to the special treatments required for AuNP modification with other materials used. In our current study, we take advantage of commercially available SPCEs that are already modified with MWCNTs, simplifying the modification process to only involve AuNP synthesis before drop-casting it onto the SPCE. Despite its simplicity, this approach yields satisfactory results in terms of surface area enhancement.

Table 3. Comparison of AuNP based modification on SPCE sensors.

Bare SPCE	Modification	Electroactive Surface Area (cm^2)	Method
SPCE from Guangdong Langyuan Biotechnology Co., Ltd.[18]	AuNP and L-Cysteine	0.049	Electrodeposition
DropSens SPCE 110[19]	AuNP and cellulose nanocrystals (CNC)	0.176 ± 0.022	Dropcasting
CH Instruments SPCE TE100[20]	Quasi-hexagonal AuNP	0.096	Dropcasting
SPCE from Palintest Limited, Gateshead, UK[21]	AuNP decorated reduced graphene oxide carbon nanotubes	0.014	Dropcasting
DropSens SPCE 110CNT	AuNP1-20/MWCNT	0.250 ± 0.007	Dropcasting

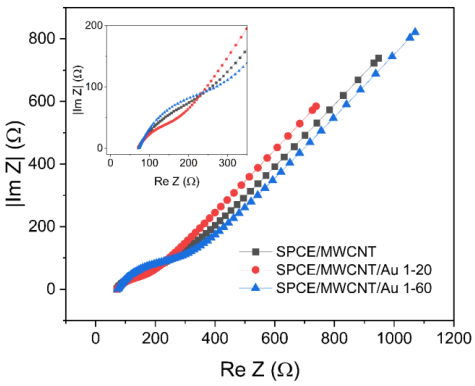

Fig. 4. Impedance Spectra of Modified and Unmodified SPCE/MWCNT with AuNP.

3.3 Impedance spectra measurement

The impedance spectra results can show how the charge transfer process occurs from the analyte to the electrode. Figure 4 shows the impedance spectra of the SPCE/MWCNT sensors before and after modification with gold nanoparticles. From the fitting results using EISyFit [22], an equivalent circuit or Randles circuit was obtained. In this circuit, the resistance of the solution between the working electrode and the reference electrode is indicated by the R_s symbol. Meanwhile, R_{ct} indicates an important process related to charge transfer that occurs between the analyte and the electrode. The amount of R_{ct} can be measured from the diameter of the semicircle in the impedance spectrum. The R_{ct} value of the SPCE/MWCNT sensor was found to be 230.50 Ω, while SPCE/MWCNT/Au 1-20 and SPCE/MWCNT/Au 1-60 were 124.62 Ω and 240.03 Ω respectively. This shows that the SPCE/MWCNT/Au 1-20 sensor has the smallest charge transfer resistance or in other words the rate of charge transfer or oxidation and reduction processes in this sensor is faster than in other sensors. This confirms the previous results from cyclic voltammetry measurements where the surface area of SPCE/MWCNT/Au 1-20 sensor turns out to be the highest.

The fitting results also show the presence of a CPE component, which accounts for the non-ideal double layer capacitance brought on by surface roughness, chemical inhomogeneity, and heterogeneity of the electrode's surface with the electrolyte as a result of ion adsorption. Meanwhile, Z_w indicates that there is a diffusion or mass transfer process in the electron transfer process of the $K_3[Fe(CN)_6]$ solution.

4 Conclusion

In this study, electroactive surface area from the largest to smallest are SPCE/MWCNT/Au 1-20 (0.250 ± 0.007 cm^2), SPCE/MWCNT (0.136 ± 0.002 cm^2), SPCE/MWCNT/Au 1-60 (0.127 ± 0.001 cm^2), and SPCE (0.108 ± 0.001 cm^2) respectively. The increase in surface area of SPCE/MWCNT/AuNP can be attributed to the availability of additional active sites provided by the AuNP. The decrease in surface area of SPCE/MWCNT/AuNP 1-60 can be the drawbacks arising from agglomeration effects. There's a good agreement between the R_{ct} of unmodified and modified SPCE with the calculated electrode surface area where modification with Au 1-20 gives the highest surface area and also the lowest R_{ct} indicating good conductivity.

Acknowledgements

This work was supported by Hibah Kolaborasi Widya Nano Sensor 2022 – 2023 organized by PT UMG IdeaLab.

References

1. Y. Wang, B. Huang, W. Dai, J. Ye, and B. Xu, J. Electroanal. Chem. **776**, 93 (2016).
2. N. Ben Messaoud, M. E. Ghica, C. Dridi, M. Ben Ali, and C. M. A. Brett, Sens. Actuators B. Chem. **253**, 513 (2017).
3. C.-J. Weng *et. al.*, J. Mater. Chem. B **1**, 4983 (2013).
4. Y. Shao et a., Microchem. J. **170**, 106726 (2021).
5. J. Shepa et al., Sensors **21**, (2021).
6. G. Paimard, E. Ghasali, and M. Baeza, Chemosensors **11**, (2023).
7. T. Hezard et al., J. Electroanal. Chem. **664**, 46 (2012).

8. F. Arduini et al., TrAC, Trends Anal. Chem. **79**, 114 (2016).
9. A. Curulli, Molecules **25**, (2020).
10. P. Jiang et al., Nanomaterials (Basel) **8**, (2018).
11. C. Guo et al., Sensors **19**, (2019).
12. D. Antuña-Jiménez, M. B. González-García, D. Hernández-Santos, and P. Fanjul-Bolado, Biosensors (Basel) **10**, (2020).
13. F. J. González-Fuentes et al., Sensors **20**, (2020).
14. J. Dong, P. L. Carpinone, G. Pyrgiotakis, P. Demokritou, and B. M. Moudgil, Kona **37**, 224 (2020).
15. W. Haiss, N. T. K. Thanh, J. Aveyard, and D. G. Fernig, Anal. Chem. **79**, 4215 (2007).
16. I. Ielo et al., Molecules **26**, (2021).
17. S. B. Aziz et al., Eng. J. **61**, 5919 (2022).
18. W. Wang et al., Biosensors (Basel) **13**, (2023).
19. D. Büyüktaş et al., Heliyon **9**, e15327 (2023).
20. A. P. M. Udayan, B. Kachwala, K. G. Karthikeyan, and S. Gunasekaran, RSC Adv **10**, 20211 (2020).
21. A. M. Musa, J. Kiely, R. Luxton, and K. C. Honeychurch, Biosensors (Basel) **13**, (2023).
22. D. Perry and M. Mamlouk, J. Power Sources 514, 230577 (2021).